

PathCRF: Ball-Free Soccer Event Detection via Possession Path Inference from Player Trajectories

Hyunsung Kim*

KAIST

Daejeon, South Korea

hyunsung.kim@kaist.ac.kr

Sang-Ki Ko

University of Seoul

Seoul, South Korea

sangkiko@uos.ac.kr

Kunhee Lee

KAIST

Daejeon, South Korea

kunhee8@kaist.ac.kr

Jinsung Yoon

Fitogther Inc.

Seoul, South Korea

jinsung.yoon@fitogther.com

Sangwoo Seo

KAIST

Daejeon, South Korea

tkddn8974@kaist.ac.kr

Chanyoung Park

KAIST

Daejeon, South Korea

cy.park@kaist.ac.kr

Abstract

Despite recent advances in AI, event data collection in soccer still relies heavily on labor-intensive manual annotation. Although prior work has explored automatic event detection using player and ball trajectories, ball tracking also remains difficult to scale due to high infrastructural and operational costs. As a result, comprehensive data collection in soccer is largely confined to top-tier competitions, limiting the broader adoption of data-driven analysis in this domain. To address this challenge, this paper proposes **PathCRF**, a framework for detecting on-ball soccer events using only player tracking data. We model player trajectories as a fully connected dynamic graph and formulate event detection as the problem of selecting exactly one edge corresponding to the current possession state at each time step. To ensure logical consistency of the resulting edge sequence, we employ a Conditional Random Field (CRF) that forbids impossible transitions between consecutive edges. Both emission and transition scores dynamically computed from edge embeddings produced by a Set Attention-based backbone architecture. During inference, the most probable edge sequence is obtained via Viterbi decoding, and events such as ball controls or passes are detected whenever the selected edge changes between adjacent time steps. Experiments show that PathCRF produces accurate, logically consistent possession paths, enabling reliable downstream analyses while substantially reducing the need for manual event annotation. The source code is available at <https://github.com/hyunsungkim-ds/pathcrf.git>.

Keywords

Sports Analytics; Event Detection; Multi-Agent Trajectory Modeling; Sequence Labeling; Conditional Random Fields

1 Introduction

The massive data collection in professional soccer has fundamentally transformed how decisions are made in this domain, shifting analysis from subjective judgments toward data-driven approaches. Contemporary soccer analytics primarily relies on two types of data [4]. The first is event data, which records on-ball actions such as passes, dribbles, and shots. The second is tracking data, which provides high-frequency spatiotemporal coordinates of all players

and the ball throughout a match. Since they capture complementary aspects of the game, comprehensive match analysis generally requires access to both data modalities.

However, acquiring both data remains costly and challenging. While recent advances in wearable and vision-based systems have made player tracking relatively inexpensive and automated, ball tracking remains substantially more expensive and difficult to scale. Due to the ball's small size, high speed, and frequent occlusions, vision-based ball tracking often suffers from missed detections or false positives, requiring dense multi-camera setups and labor-intensive manual corrections [53, 63, 72, 74]. Sensor-based solutions [27, 55] further raise deployment costs, as they require meticulous calibration and expensive stadium-wide infrastructure.

In parallel, even in the era of advanced AI, event data collection still relies heavily on manual annotation. Human annotators must watch entire matches and record every event's timestamp, location, involved players, and category. Several studies [8, 47, 70] have attempted to automatically detect events from player and ball trajectories, but they still depend on accurate ball tracking, limiting their scalability. Consequently, pipelines for collecting complete sets of event and tracking data remain largely confined to top-tier competitions, and have not scaled to lower or youth divisions.

To overcome these limitations, prior work has explored inferring ball-related information directly from player trajectories. Kim et al. [37] and Capellera et al. [10, 12] infer ball positions or classify ball states using only player trajectories. However, these approaches do not explicitly enforce physical constraints, often producing implausible ball trajectories or unrealistically frequent possession changes. Other studies [60, 61] incorporate visual cues such as player image crops extracted from video to improve accuracy, but they use tactical camera footage that always capture the entire pitch, which is substantially harder to obtain than standard broadcasting video or tracking data. This requirement runs counter to the goal of democratizing automated data collection across lower-tier competitions.

In this paper, we propose **PathCRF**, a framework for detecting on-ball soccer events solely from player trajectories. Rather than estimating ball positions or identifying ball states, we formulate event detection as the problem of inferring a *possession path*, indicating how the ball moves between players over time. To this end, player trajectories are represented as a fully connected dynamic

*Also with Fitogther Inc..

graph, and at each time step the model selects exactly one edge corresponding to the current possession state: a self-loop for dribbling, or a directed sender-receiver edge for a kick in flight.

To ensure that the inferred possession path is logically consistent, we construct a Conditional Random Field (CRF) [41] on top of a neural backbone. The backbone jointly encodes the dynamic interactions between players over time via socio-temporal attention [43] and produces a sequence of candidate edge embeddings. The CRF dynamically computes emission and transition scores from these edge embeddings, where logically impossible edge-to-edge transitions are masked with a large negative scores so that any sequence containing illegal transitions is assigned a very low likelihood. At inference time, the most probable sequence is obtained via Viterbi decoding [71], and on-ball events are detected whenever the selected edge changes between consecutive time steps.

Experimental results show that PathCRF identifies the correct possession edge among $26^2 = 676$ candidate edges with an accuracy of 69.64%, and achieves F1-score of 75.69% in event detection. Furthermore, we show that a wide range of downstream metrics, including event heatmaps, team possession statistics, and pass networks, are closely approximated using the detected events, facilitating reliable match analysis without manual event annotation.

In summary, this paper proposes a framework for detecting on-ball soccer events using only player tracking data, without requiring expensive ball-tracking hardware or labor-intensive annotation. The main contributions are as follows:

- Formulating soccer event detection as a sequential edge selection problem over a dynamic graph.
- Introducing neural CRF-based sequence inference, used primarily in natural language processing (NLP), into sports analytics to enforce domain-specific physical constraints.
- Demonstrating that key event-based analytics, including spatial tendencies, team possession statistics, and passing patterns, can be reliably approximated without manual event annotation.
- Releasing the source code using publicly available tracking data [5], so that anyone can easily reproduce the results.

2 Proposed Framework

In this section, we formulate soccer event detection as a path inference problem over a fully connected dynamic graph (Section 2.1) and present a framework consisting of a neural backbone (Section 2.2), a Dynamic Masked Conditional Random Field (CRF) (Section 2.3), and an event detection mechanism (Section 2.4). The overall architecture is illustrated in Figure 1.

2.1 Problem Formulation

Our ultimate objective is to detect on-ball soccer events using only player tracking data. To this end, we model player trajectories as a fully connected dynamic graph and formulate event detection as the problem of inferring a *possession path*, represented as a sequence of edges that describe the ball possession states over time.

Formally, given a set of player trajectories $X_{1:T} = \{\mathbf{x}_{v,1:T}\}_{v \in \mathcal{V}}$, we represent each snapshot as a fully connected directed graph over the extended node set $\widetilde{\mathcal{V}}$. This set is defined as the union of the player set \mathcal{V} and the set O of four *outside* nodes, each corresponding to the ball leaving the pitch through one of the four boundary lines

(left, right, top, and bottom)¹. Then, the ball possession state at each time step t corresponds to exactly one edge $e_t = (u_t, v_t)$ between nodes in $\widetilde{\mathcal{V}}$, where a self-loop (u_t, u_t) indicates that the player u_t is in control of the ball, while a directed edge (u_t, v_t) with $u_t \neq v_t$ represents the ball traveling from sender u_t to receiver v_t .

The goal of the model is therefore to select the edge sequence $\hat{e} = (\hat{e}_1, \dots, \hat{e}_T)$ indicating the ball possession path from player trajectories alone. Once the possession path is obtained, on-ball events are detected by identifying time steps where the selected edge changes, i.e., $\hat{e}_{t-1} \neq \hat{e}_t$. Each detected event is then categorized according to the type of the newly selected edge, yielding *control*, *kick*, or *out-of-play* events (see Section 2.4 for details).

2.2 Backbone Architecture

To extract rich socio-temporal representations of player interactions, we adopt an encoder design inspired by ROLAND [77] that combines social module to capture multi-agent interactions and a temporal module to encode sequential dependencies. Following TranSPORTmer [10], we stack two of these encoders to progressively refine the game contexts from coarse to fine levels. The resulting node embeddings are subsequently transformed into edge embeddings, which serve as the fundamental features for scoring edge sequences in the CRF described in Section 2.3.

2.2.1 Socio-temporal encoder blocks. Let $\mathbf{H}_t^{(l-1)} \in \mathbb{R}^{|\widetilde{\mathcal{V}}| \times d}$ denote the input node features for the l -th encoder at time t ($l = 1, 2$), where $\mathbf{H}_t^{(0)} = \mathbf{X}_t = \{\mathbf{x}_{v,t}\}_{v \in \widetilde{\mathcal{V}}}$. Each encoder consists of a social module followed by a temporal module, jointly capturing spatial interactions among players and their evolution over time.

Social module. Following Kim et al. [37], we model multi-agent interactions at each time step using a combination of a partially permutation-equivariant (PPE) network and a fully permutation-equivariant (FPE) network. The PPE encoder processes nodes within each group (i.e., either team or the set of outside nodes) separately using an Induced Set Attention Block (ISAB) [43] to capture intra-group dynamics, respecting the fact that players within a team are semantically unordered yet distinct from those in the opposing team. Complementarily, the FPE module processes all nodes through a single ISAB to encode global inter-group contexts. The outputs of these PPE and FPE networks are concatenated to form node representations for the snapshot at t :

$$\tilde{\mathbf{H}}_t^{(l)} = \{\tilde{\mathbf{h}}_{v,t}^{(l)}\}_{v \in \widetilde{\mathcal{V}}} = [\text{PPE}(\mathbf{H}_t^{(l-1)}) ; \text{FPE}(\mathbf{H}_t^{(l-1)})] \in \mathbb{R}^{|\widetilde{\mathcal{V}}| \times d}. \quad (1)$$

Temporal module. The temporal module aggregates node representations across time to capture the evolution of interactions:

$$\mathbf{h}_{v,1:T}^{(l)} = \text{Temporal}(\tilde{\mathbf{h}}_{v,1:T}^{(l)}) \in \mathbb{R}^{T \times d}, \quad (2)$$

which yields the node embeddings $\mathbf{H}_t^{(l)} = \{\mathbf{h}_{v,t}^{(l)}\}_{v \in \widetilde{\mathcal{V}}}$ that serve as the input for the next stage. In principle, this module can be instantiated with any sequence model, but in this work, we adopt the architecture proposed in TranSPORTmer [10] that combines positional encoding (PE) [69] with stacked Set Attention Blocks (SABs) [43] as a concrete instantiation.

¹Since $|\mathcal{V}| = 22$ in standard soccer matches without red cards, the total number of nodes is $|\widetilde{\mathcal{V}}| = 26$ in most cases.

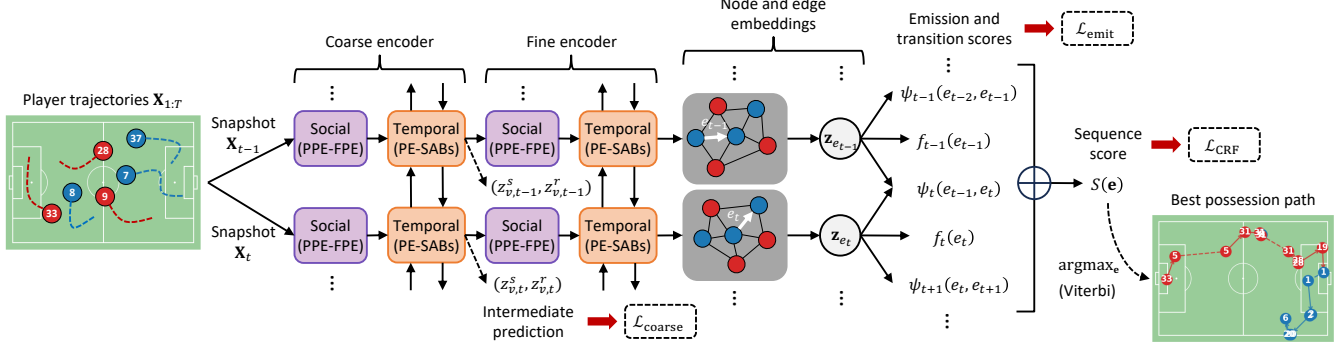


Figure 1: Overall architecture of PathCRF.

Empirically, in Section 3.5, we observe that this attention-based temporal module achieves performance comparable to its Bi-LSTM [30] counterpart. We attribute this behavior to the nature of our task: soccer possession dynamics are largely driven by short-term continuity, where the most recent context is typically the most informative. As a result, both recurrent models with an explicit recency bias and attention-based models that learn which time steps to focus on tend to yield similar performance in this setting.

2.2.2 Intermediate supervision. To encourage the backbone to learn possession-related semantics early in the network, we introduce an auxiliary supervision task using intermediate node embeddings $H_t^{(1)}$ produced by the first (coarse) encoder, inspired by prior work [37, 78]. Specifically, each node embedding $h_{v,t}^{(1)} \in \mathbb{R}^d$ is projected into a two-dimensional vector comprising a sender logit and a receiver logit via a Multilayer Perceptron (MLP):

$$(z_{v,t}^s, z_{v,t}^r) = \text{MLP}_{\text{coarse}} \left(h_{v,t}^{(1)} \right) \in \mathbb{R}^2. \quad (3)$$

We then apply the softmax normalization across all nodes for the sender and receiver logits, respectively, to obtain the probabilities of each node being the sender or the receiver of the ball at time t . The cross-entropy loss between these probabilities and the ground-truth sender/receiver labels is incorporated as an auxiliary term into the final training objective detailed in Section 2.3.3.

2.2.3 Edge embedding construction. From the second (fine) encoder, we obtain refined node embeddings $H_t^{(2)} = \{h_{v,t}^{(2)}\}_{v \in \mathcal{V}}$. To transition from node-level representations to candidate possession states, we construct an embedding for each directed edge $e = (u, v)$ by concatenating the embeddings of its source (sender) and destination (receiver) nodes, followed by an MLP:

$$z_{e,t} = \text{MLP}_{\text{edge}} \left(\left[h_{u,t}^{(2)}, h_{v,t}^{(2)} \right] \right) \in \mathbb{R}. \quad (4)$$

These edge embeddings serve as the core features used to compute the CRF scores described in Section 2.3.1.

2.3 Dynamic Masked Conditional Random Field

Given the edge embeddings $z_{e,t}$ produced by the backbone, a straightforward approach to infer a possession path is to compute edge logits independently at each time step and form a sequence by selecting the highest-scoring edge via an argmax operation. However, such per-time-step classification ignores semantic dependencies

between consecutive possession states, often producing logically inconsistent edge sequences. For instance, a model might select a self-loop for player u at time t and immediately predict another edge (v, w) where $u \neq v$ at time $t + 1$ without any intermediate pass edge (u, v) , implying a physically impossible “teleportation” of the ball. (See the red-highlighted players in Figure 2b.) To resolve this, we employ a Conditional Random Field (CRF) [41] to strictly enforce domain-specific transition constraints.

2.3.1 Scoring edge sequences. Unlike the independent classification approach that assign a probability to each edge per time step, the CRF framework models the probability of the entire edge sequence $\mathbf{e} = (e_1, \dots, e_T)$ given the input observations $\mathbf{X} = \mathbf{X}_{1:T}$. The probability of a sequence \mathbf{e} is defined as

$$p(\mathbf{e}|\mathbf{X}) = \frac{\exp(S(\mathbf{e}))}{\sum_{\mathbf{e}'} \exp(S(\mathbf{e}'))} \quad (5)$$

where $S(\mathbf{e})$ is the score of the sequence, computed as the sum of emission and transition scores over all time steps:

$$S(\mathbf{e}) = f_1(e_1) + \sum_{t=2}^T (f_t(e_t) + \psi_t(e_{t-1}, e_t)). \quad (6)$$

The emission score $f_t(e_t)$ indicates the local likelihood of edge e_t being the current possession state. We compute this score by projecting the edge embedding $z_{e,t}$ obtained from Eq. 4:

$$f_t(e) = \text{MLP}_{\text{emit}}(z_{e,t}) \in \mathbb{R}. \quad (7)$$

The transition score $\psi_t(e_{t-1}, e_t)$ measures the possibility of transitioning from the previous edge e_{t-1} to the current edge e_t . Standard CRFs typically parameterize this score using a static transition matrix Ψ , where each entry ψ_{ij} is a learnable weight representing the likelihood of transition from state i to j [33, 52].

However, this static parametrization is ill-suited for capturing the time-varying nature of game dynamics. For instance, consider a long pass corresponding to the directed edge (u, v) . In the early phase of the pass, the probability of the identity transition $(u, v) \rightarrow (u, v)$ should be high as the ball is likely to be still traveling toward the receiver. As time progresses and the ball approaches the receiver v , however, the likelihood of transitions into a reception state such as (v, v) and (v, w) should increase. A static transition matrix cannot adapt to such evolving spatiotemporal context.

To address this limitation, we compute transition scores *dynamically* from edge embeddings produced by the backbone. Specifically,

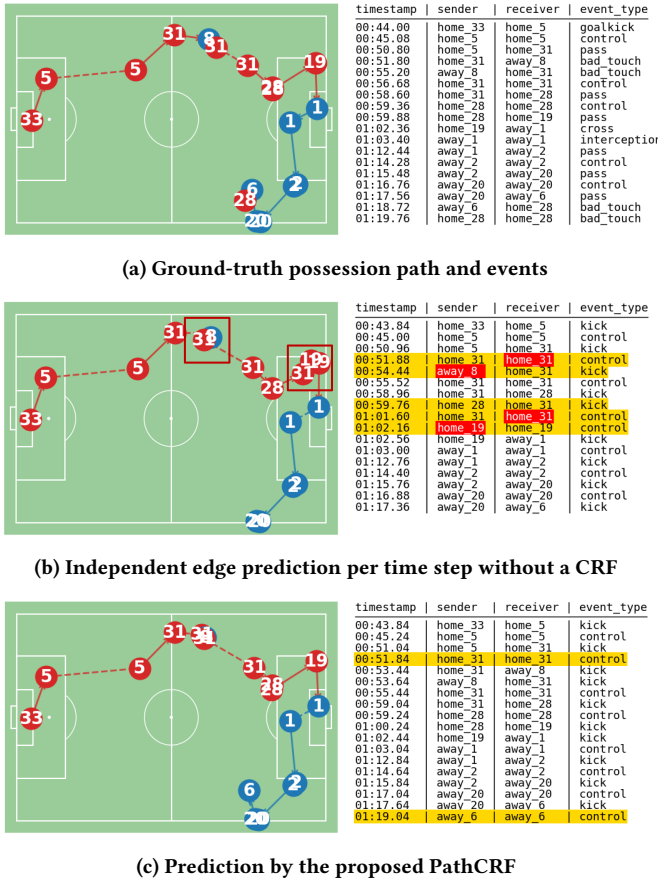


Figure 2: Comparison of the ground-truth possession path and events with model predictions on an in-play segment of the test dataset. Predicted events with incorrect sender or receiver attributes are highlighted in yellow, and physically impossible transitions are highlighted in red.

for a given transition from edge e' at $t-1$ to edge e at t , we concatenate their embeddings and pass them through a shared MLP:

$$\psi_t(e', e) = \text{MLP}_{\text{trans}}([\mathbf{z}_{e', t-1}; \mathbf{z}_{e, t}]) \in \mathbb{R}. \quad (8)$$

This allows the transition scores to adapt to the evolving game context at each time step, thereby improving the event detection performance as discussed in Section 3.4.

2.3.2 Masking impossible transitions. Another key feature of our approach is the imposition of hard constraints on these transition scores. First, we define the *set of allowed transitions* \mathcal{A} as the union of the following subsets:

- $\mathcal{A}^{\text{id}} = \{(u, v) \rightarrow (u, v) : u, v \in \mathcal{V}\}$, representing the continuation of the current state,
- $\mathcal{A}^{\text{kick}} = \{(u, u) \rightarrow (u, v) : u \in \mathcal{V}, v \in \mathcal{V}, u \neq v\}$, representing a player u releasing the ball to pass to v ,
- $\mathcal{A}^{\text{rec}} = \{(u, v) \rightarrow (v, w) : u, v \in \mathcal{V}, w \in \mathcal{V}, u \neq v\}$, representing the receiver v either controlling the ball ($w = v$) or making a one-touch kick ($w \neq v$), and

- $\mathcal{A}^{\text{out}} = \{(u, o) \rightarrow (o, o) : u \in \mathcal{V}, o \in \mathcal{O}\}$, representing the ball going out of play².

Then, following the strategy of Masked CRF [73], we mask all transitions except for those in \mathcal{A} by a fixed, large negative score (e.g., -10^4). This mechanism effectively prunes illegal paths from the search space and forces the model to produce only logically consistent sequences.

2.3.3 Model training. We train the entire framework end-to-end by minimizing the negative log-likelihood of the ground-truth edge sequence $\mathbf{e}^* = (e_1^*, \dots, e_T^*)$ given the input trajectories \mathbf{X} :

$$\mathcal{L}_{\text{CRF}} = -\log p(\mathbf{e}^* | \mathbf{X}) = \log Z - S(\mathbf{e}^*) \quad (9)$$

where $S(\mathbf{e}^*)$ is the score of the ground-truth sequence computed by Eq. 6 and $Z = \sum_{\mathbf{e}'} \exp(S(\mathbf{e}'))$ is the partition function that normalizes the probability distribution. Following the standard formulation of CRFs [41], we efficiently compute $\log Z$ using the forward algorithm based on dynamic programming, where the detailed procedure is elaborated on Appendix A.1.

To further stabilize training and encourage discriminative feature learning, we add two auxiliary loss terms to the training objective: the *intermediate classification loss* $\mathcal{L}_{\text{coarse}} = \mathcal{L}_{\text{coarse}}^s + \mathcal{L}_{\text{coarse}}^r$ described in Section 2.2.2 and the *emission classification loss* $\mathcal{L}_{\text{emit}}$, which computes the cross-entropy between the emission logits $f_t(e)$ and the true possession state e_t^* . The final objective is constructed as a weighted sum of the three loss terms:

$$\mathcal{L} = \mathcal{L}_{\text{CRF}} + \lambda_1 \mathcal{L}_{\text{coarse}} + \lambda_2 \mathcal{L}_{\text{emit}}, \quad (10)$$

where λ_1 and λ_2 are hyperparameters balancing the contributions of the auxiliary terms.

2.3.4 Viterbi decoding. During the inference phase, the CRF framework identifies the single most likely edge sequence $\hat{\mathbf{e}} = \arg \max_{\mathbf{e}} S(\mathbf{e})$ using the Viterbi algorithm [41, 71]. By incorporating the hard constraints described in Section 2.3.2, the decoding process automatically prunes impossible transitions from the search space, ensuring that the inferred path is logically consistent with all transitions belonging to \mathcal{A} . For further details, see Appendix A.2.

2.4 Event Detection

Once the best edge sequence $\hat{\mathbf{e}} = (\hat{e}_1, \dots, \hat{e}_T)$ is obtained via Viterbi decoding, we deterministically extract discrete soccer events by identifying time steps where the possession state changes (i.e., $\hat{e}_{t-1} \neq \hat{e}_t$). At each change-point t , the detected event is categorized based on the topology of the initiated edge \hat{e}_t as follows:

- **Control:** A ball control is detected at time t when the state transitions to a player self-loop (u, u) with $u \in \mathcal{V}$ at t .
- **Kick:** A kick is detected at time t when a state changes to an edge (u, v) with $u \in \mathcal{V}, v \in \mathcal{V}, u \neq v$ at t . Note that this event can occur immediately after a ball control by u (controlled kick) or a kick towards u (one-touch kick).
- **Out-of-play:** An out-of-play event is detected when the state transitions to an outside node self-loop (o, o) with $o \in \mathcal{O}$ at t , indicating the ball has crossed the pitch boundary.

²Since we perform training and inference only on windows inside in-play segments as described in Section 3.1, the self-loop (o, o) of each outside node $o \in \mathcal{O}$ serves as an absorbing state of our edge-to-edge transition system.

Figure 2c visualizes a representative example of the inferred possession path and the corresponding events detected by our framework. In contrast to the non-CRF baseline in Figure 2b, which produces illegal transitions where the receiver of the previous event does not match the sender of the next event (red-highlighted case), PathCRF explicitly enforces transition constraints that guarantee a globally consistent possession sequence. Moreover, our dynamic estimation of emission and transition scores not only eliminates such impossible event patterns but also improves prediction accuracy, yielding fewer mislabeled events as indicated by the reduced proportion of yellow-highlighted errors compared to Figure 2b. Overall, PathCRF effectively segments continuous game flow into on-ball events solely from player trajectories.

3 Experiments

In this section, we evaluate PathCRF through extensive experiments on publicly available soccer tracking data [5]. Section 3.1 describes the dataset and the preprocessing pipeline. Section 3.2 and Section 3.3 introduce baseline methods and evaluation metrics, respectively. Section 3.4 reports the main experimental results, and Section 3.5 provides an ablation study on backbone design choices.

3.1 Data Preparation

As professional soccer clubs and data providers typically keep tracking data proprietary, complete sets of event and tracking data are rarely publicly available. To ensure full reproducibility, we conduct experiments exclusively on the Sportec Open DFL Dataset [5], which provides high-quality event and tracking data from seven matches of German Bundesliga 1 and 2. Despite the limited scale of the data, we observe that PathCRF achieves strong performance even when trained on only five matches, as reported in Section 3.4.

As the manual annotations often contain imprecise timestamps, we synchronize event timing based on player and ball trajectories using ELASTIC [38]. In addition, since the raw event data miss some ball touches, we detect abrupt directional changes in the ball trajectory using the Ramer–Douglas–Peucker (RDP) algorithm [22, 62] as candidate ball-touch points. Then, we align them with the synchronized events via the Needleman–Wunsch algorithm [57], and insert unmatched points as additional ball-touch events. Finally, from this refined set of events, we general ground-truth edge labels indicating the possession state per time step.

We restrict training and inference to in-play segments, since no on-ball events occur during stoppages. Following prior work [37], we define each continuous in-play segment as an *episode*, and apply 10-second sliding windows with a stride of 5 frames in each episode when constructing the training dataset. The tracking data are downsampled from 25 FPS to 5 FPS for computational efficiency, resulting in 50 time steps per window, and predictions are later upsampled to 25 FPS for downstream analyses. Dataset statistics are summarized in Table 1.

3.2 Baseline Methods

We compare the proposed framework against a range of baselines to evaluate the impact of structured inference, dynamic transition scoring, and explicit masking of illegal transitions. All baselines share the same backbone architecture described in Section 2.2.

Table 1: Statistics of the dataset splits.

Split	Matches	Episodes	Events	Frames	Windows
Train.	5	379	8,792	364,003	54,683
Valid.	1	71	1,902	80,076	12,620
Test	1	91	1,831	85,304	—

- **Ball Trajectory Postprocessing (Ball TP):** A two-stage pipeline that first regresses the 2D ball trajectory from player tracking data, and then detect ball possession using the rule-based heuristics proposed in Ball Radar [37].
- **Non-CRF:** The backbone is trained only with cross-entropy losses (i.e., $\mathcal{L}_{\text{coarse}}$ and $\mathcal{L}_{\text{emit}}$ in Eq. 10), and the possession path is obtained by independently selecting the edge with the highest logit at each time step.
- **Greedy Constrained Decoding (GCD):** Uses the same Non-CRF model as above, but greedily enforces transition constraints at inference time. The first time step selects the argmax edge in terms of output logit, and each subsequent step selects the argmax edge only among those reachable from the previously selected edge under the transition rules defined in Section 2.3.2.
- **Viterbi Constrained Decoding (VCD):** Uses the same Non-CRF model as above, but applies Viterbi decoding [71], obtaining the globally optimal sequence while satisfying the predefined transition constraints.
- **Static Dense CRF:** A standard CRF with a static, dense transition matrix learned independently of the input, without masking illegal transitions [33].
- **Static Masked CRF:** A static CRF that explicitly masks predefined illegal transitions [73].
- **Dynamic Dense CRF:** Computes transition scores dynamically from pairs of edge embeddings, but does not mask illegal transitions.
- **Dynamic Masked CRF (ours):** Combines dynamic transition scoring with explicit masking of illegal transitions.

3.3 Evaluation Metrics

We evaluate the proposed framework at both the edge level and the event level to assess the quality of the inferred possession paths and the resulting on-ball events.

Edge-level metrics. At the edge level, we evaluate the predicted possession states at each time step by reporting *sender accuracy*, *receiver accuracy*, and *edge accuracy*, where the edge accuracy requires correctly selecting both the sender and receiver. In addition, we measure the *violation rate*, defined as the percentage of illegal transitions in the predicted edge sequence.

Event-level metrics. At the event level, we evaluate event detection performance using *precision*, *recall*, and *F1-score*. To compute these metrics, we align the detected and ground-truth event sequences using the Needleman–Wunsch algorithm [57], and count a detected event as correct if it is matched with a true event having (i) the same event type, (ii) the same acting player, and (iii) a temporal difference within one second. Since the ground-truth events follow the SPADL schema [17] with fine-grained event types, we map

Table 2: Performance comparison of baseline methods on the test data.

Structuring method	Edge accuracy	Sender accuracy	Receiver accuracy	Violation rate	Event precision	Event recall	Event F1
Ball TP	47.01%	58.58%	67.01%	0.00%	44.64% (967/2166)	52.81% (967/1831)	48.39%
Non-CRF	69.24%	79.78%	81.62%	2.80%	58.77% (1347/2292)	73.57% (1347/1831)	65.34%
Non-CRF & GCD	66.34%	76.89%	78.19%	0.00%	68.81% (1339/1946)	73.13% (1339/1831)	70.90%
Non-CRF & VCD	69.68%	80.16%	<u>81.97%</u>	0.00%	69.50% (1413/2033)	77.17% (1413/1831)	73.14%
Static Dense CRF	69.41%	80.59%	81.61%	2.18%	62.54% (1399/2237)	76.41% (1399/1831)	68.78%
Static Masked CRF	69.54%	80.29%	82.02%	0.00%	68.57% (1464/2135)	79.96% (1464/1831)	<u>73.83%</u>
Dynamic Dense CRF	69.08%	79.56%	81.95%	2.28%	61.75% (1377/2230)	75.20% (1377/1831)	67.82%
Dynamic Masked CRF	69.64%	80.44%	82.28%	0.00%	73.18% (1435/1961)	78.37% (1435/1831)	75.69%

Table 3: Backbone design ablation study on the test data.

Social module	Temporal module	Structuring method	Edge accuracy	Sender accuracy	Receiver accuracy	Violation rate	Event precision	Event recall	Event F1
SAB (TranSPORTmer)	PE-SABs (TranSPORTmer)	Non-CRF	58.49%	70.98%	73.84%	4.45%	46.14% (1107/2399)	60.46% (1107/1831)	52.34%
		Non-CRF & VCD	59.08%	71.71%	74.29%	0.00%	59.41% (1237/2082)	67.56% (1237/1831)	63.23%
		Dynamic MCRF	62.97%	74.91%	77.98%	0.00%	66.51% (1281/1926)	69.96% (1281/1831)	68.19%
PPE-FPE (Ball Radar)	Bi-LSTM (Ball Radar)	Non-CRF	69.15%	80.01%	81.01%	2.17%	61.50% (1337/2174)	73.02% (1337/1831)	66.77%
		Non-CRF & VCD	69.32%	80.22%	81.15%	0.00%	68.89% (1382/2006)	75.48% (1382/1831)	72.04%
		Dynamic MCRF	70.39%	80.98%	82.30%	0.00%	72.67% (1428/1965)	<u>77.99%</u> (1428/1831)	<u>75.24%</u>
PPE-FPE (Ball Radar)	PE-SABs (TranSPORTmer)	Non-CRF	69.24%	79.78%	81.62%	2.80%	58.77% (1347/2292)	73.57% (1347/1831)	65.34%
		Non-CRF & VCD	69.68%	80.16%	81.97%	0.00%	69.50% (1413/2033)	77.17% (1413/1831)	73.14%
		Dynamic MCRF	69.64%	80.44%	82.28%	0.00%	73.18% (1435/1961)	78.37% (1435/1831)	75.69%

them into the three simplified categories defined in Section 2.4 for consistent matching.

3.4 Main Results

Table 2 compares baseline methods at both the edge and event levels, where the best and runner-up results are highlighted in **bold** and underline, respectively. Since all methods share the same backbone, edge-level accuracies are largely similar except for Ball TP. However, event-level performance varies significantly, underscoring the importance of structured inference for reliable event detection.

First, Ball TP performs markedly worse than edge-based approaches. Although it predicts ball trajectories with a localization error of 2.74 m, it assigns possession states only through heuristic postprocessing (e.g., using ball acceleration and player-to-ball distance). This leads to a notable drop in event detection quality, which motivates our edge inference formulation.

The Non-CRF baseline, which selects edges independently per time step, produces 2.80% illegal transitions and over-segments the sequence, leading to many spurious event detections and low precision (58.77%). In contrast, simply applying constrained decoding at inference time entirely eliminates violations and improves event precision by more than 10%^p (i.e., up to 68.81% for GCD and 69.50% for VCD), demonstrating that enforcing transition constraints is critical for reliable event detection. Moreover, VCD slightly outperforms GCD, indicating the advantage of globally optimizing the entire sequence under constraints than greedy local decisions.

Compared to constrained decoding, Masked CRFs further improve performance by incorporating constraints during training. While constrained decoding has become more prevalent in recent

NLP due to the huge cost of fine-tuning LLMs and the complexity of linguistic constraints [28, 31, 49, 67], our setting differs in that models can be efficiently trained from scratch and the governing constraints are simple (as explicitly defined in Section 2.3.2), making CRF-based training both feasible and advantageous.

Lastly, the comparison between CRF variants highlights the necessity of explicit violation masking and dynamic transition scoring. Specifically, Dense CRFs without masking still produce illegal transitions and perform much worse in event detection than masked variants. Furthermore, Dynamic Masked CRF achieves a much higher event precision (73.18%) than Static Masked CRF (68.57%). This is because static transition matrices always assign non-negligible probabilities to unnecessary state changes, resulting in far more frequent event detections (2,135) than the ground truth (1,831). In contrast, Dynamic Masked CRF adapts the likelihood of maintaining the current state to the context, yielding a more realistic number of events (1,961) and thereby improving the F1-score.

3.5 Ablation Study on Backbone Design

To better understand how different backbone designs affect the performance, we conduct an ablation study by combining components proposed in two recent sports trajectory modeling frameworks: Ball Radar [37] and TranSPORTmer [10]. Specifically, Ball Radar employs a social module combining PPE and FPE networks based on ISABs [43] described in Section 2.2.1 with a temporal module using Bi-LSTM [30]. Meanwhile, TranSPORTmer uses a vanilla SAB [43] social module and an attention-based temporal module consisting of positional encoding (PE) [69] and stacked SABs.

Based on these components, Table 3 compares three variants:

- The TranSPORTmer backbone (SAB & PE-SABs)
- The Ball Radar backbone (PPE-FPE & Bi-LSTM)
- Our hybrid backbone, which adopts the Ball Radar’s social module (PPE-FPE) but replaces the temporal module with TranSPORTmer’s encoder (PE-SABs). As described in Section 2.2.1, this configuration is used as the main backbone architecture throughout the paper.

The results show that replacing the TranSPORTmer’s SAB-based social module with Ball Radar’s PPE-FPE consistently yields a substantial improvement, indicating that explicitly separating intra-team interactions (PPE) and global cross-team contexts (FPE) provides a stronger inductive bias than treating all agents uniformly with a single SAB. In contrast, once PPE-FPE is adopted, the choice of temporal module between Bi-LSTM and PE-SABs has only a marginal impact, where Bi-LSTM slightly improves edge-level accuracies and PE-SABs achieves slightly better event-level performance. This suggests that soccer possession dynamics are largely governed by short-term continuity, where recent context is often the most informative, making both recurrent and attention-based temporal modules similarly effective in this task.

4 Practical Applications

In this section, we showcase a wide range of practical applications of the proposed PathCRF. First, we demonstrate that PathCRF can closely approximate diverse downstream analyses without requiring any manual event annotation, including spatial event heatmaps (Section 4.1), team possession statistics (Section 4.2), and pass networks (Section 4.3). Furthermore, when completely accurate event data are still required for fine-grained scene analysis, Section 4.4 discusses how our framework can substantially reduce human workload by supporting semi-automated event data collection.

4.1 Spatial Distribution of On-Ball Plays

Since the spatial distribution of on-ball plays reflects team tactics and individual playing styles, we examine whether PathCRF can accurately reproduce these positional tendencies from detected events. As shown in Figure 3, the predicted heatmaps for both teams and individual players closely align with the true heatmaps, implying that PathCRF preserves positional patterns of events with high fidelity. This suggests that a wide range of downstream analyses for characterizing the playing styles at both the team [19, 51] and player levels [18, 20] can be directly applied to our detected events, enabling scalable event-based soccer analytics without manual tagging.

4.2 Team Possession Statistics

Team-level possession share is one of the most widely used indicators in both broadcasting and analytics, as it provides a simple yet informative summary of which team controlled the flow of the match. We therefore examine whether team possession can be accurately recovered using only the events detected by PathCRF.

On the test match, the ground-truth possession share of the home team is 62.13%, while our prediction yields 62.64%, showing that PathCRF can approximate overall possession statistics with near-perfect accuracy. Interestingly, although the frame-level team possession classification accuracy is 92.40%, misclassifications occur for both teams and tend to cancel out over time, resulting in an

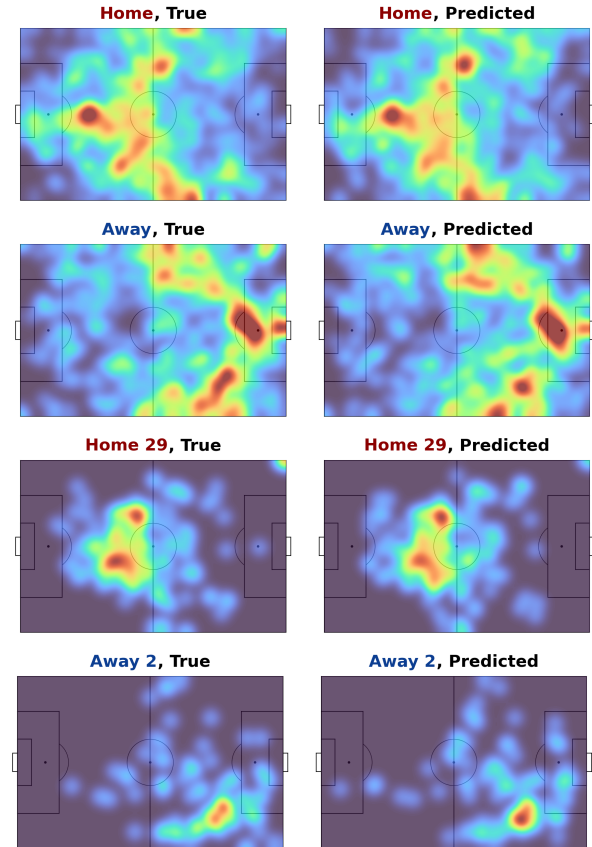


Figure 3: Comparison of kernel density estimation (KDE) heatmaps computed from true and detected events, for both teams and the most event-involved player from each team.

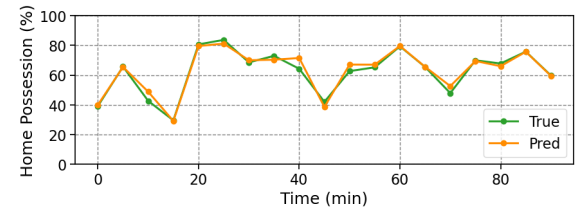


Figure 4: 5-minute timeline of home team’s possession shares computed from true and detected events, respectively.

even more accurate estimate of the cumulative possession share. This is also reflected in the home team’s possession timeline in Figure 4, where the predicted values closely track the ground truth even at a fine granularity of 5-minute intervals.

These results indicate that match dominance can be reliably analyzed using only player tracking data and PathCRF. Moreover, we expect that accurate team possession segmentation enables richer contextual analyses without manual annotation, such as separating offensive and defensive phases when calculating physical performance metrics [9, 36, 39] or estimating team formations [6, 40].

Table 4: Similarity between ground-truth and predicted pass networks at node degree, edge weight, and graph levels.

Team	Node degree		Edge weight		Graph structure	
	True mean	MAE	True mean	MAE	JSD	Spectral
Home	45.19	2.64	5.18	1.08	0.0228	0.0270
Away	24.27	2.73	3.26	1.05	0.0552	0.0138

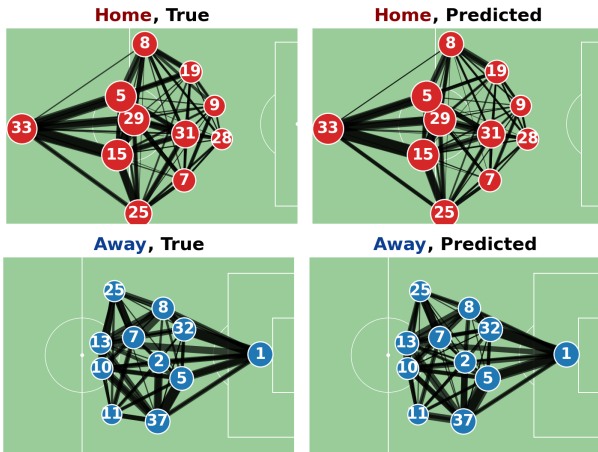


Figure 5: Visual comparison of pass networks constructed from ground-truth and detected events.

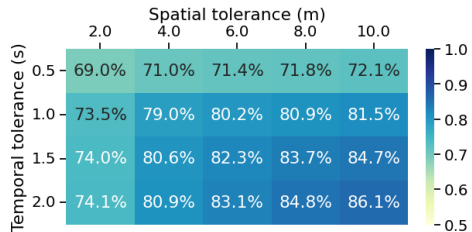


Figure 6: Event recall under varying tolerance thresholds.

4.3 Pass Networks

Pass networks are a widely used representation for analyzing team's collective passing structures, and have been extensively studied in soccer analytics literature [15, 16, 23, 48]. To examine whether PathCRF enables such analyses without manual pass annotation, we construct pass networks from the detected kick events and compare them against those derived from ground-truth event data.

Figure 5 visualizes the resulting networks for both teams. Each node is positioned at the player's average location and its size is proportional to the number of successful outgoing passes, where each pair of substituted players are merged as a single node. Edge thickness represents the number of completed passes between the pair of nodes. As shown, the predicted pass networks closely match the ground-truth networks in terms of both the overall passing structure and the key hubs responsible for ball circulation, indicating that PathCRF reliably captures team-level ball flow patterns.

To quantitatively evaluate the similarity between the true and predicted pass networks, we measure how similar they are at the

node, edge, and graph levels. Specifically, we compare (i) node degrees and (ii) edge weights using mean absolute error (MAE), and additionally measure (iii) graph-level structural similarity using Jensen-Shannon divergence (JSD) [46] and spectral distance [14]. As reported in Table 4, the MAE values for both node degree and edge weight are small relative to the true mean degrees and weights, respectively, indicating that PathCRF accurately recovers the key passing frequencies. Moreover, both JSD and spectral distance are close to zero, implying that the predicted networks preserve the global structure of team passing patterns. These results demonstrate that diverse downstream analyses, such as quantifying player contributions [23], team strategies [48], and team performance [15, 16], can be reliably conducted using detected events.

4.4 Semi-Automated Event Data Collection

Although the events detected by PathCRF can closely approximate various downstream metrics, some fine-grained scene analyses may still require near-perfect event-level accuracy. In such cases, instead of manually annotating every event and its attributes from scratch, we propose a human-in-the-loop data collection pipeline where annotators verify and correct model-generated events, substantially reducing the labor cost.

Importantly, even when the predicted player identity is incorrect, PathCRF often localizes the event timing and location accurately. To quantify this, we measure recall under relaxed matching criteria, where a detected event is considered correct if its timestamp and location fall within predefined temporal and spatial tolerance thresholds of the aligned ground-truth event. As shown in Figure 6, PathCRF achieves nearly 80% recall even a relatively strict criterion of 1 s and 4 m, which further increases to 86.1% when allowing discrepancies up to 2 s and 10 m. These results suggest that many mismatches are near-misses rather than complete failures, which remain useful in practice as they only require correcting a subset of event attributes rather than annotating the entire event records.

Overall, this demonstrates that PathCRF can serve not only as a tool for fully automated event-based analysis, but also as an effective pre-annotation system that significantly streamlines the collection of high-quality soccer event data.

5 Conclusion

In this paper, we propose PathCRF, a framework for detecting on-ball soccer events using only player tracking data. By formulating event detection as a sequential edge selection problem over a fully connected dynamic graph and enforcing hard constraints on edge-to-edge transitions via a dynamic masked CRF, the framework produces logically consistent possession sequences and achieves strong event-level performance. Moreover, we demonstrated that the detected events can reliably support various downstream analyses, highlighting the practical value of PathCRF as a scalable alternative to expensive ball tracking systems and labor-intensive manual event annotation.

As future work, we aim to further improve detection accuracy by integrating additional sources of inductive bias, such as partial human guidance for ambiguous events or prior knowledge of player-specific behavioral tendencies. We also plan to incorporate visual features from easily accessible broadcast videos into the model.

Leveraging such multi-modal information could not only enhance robustness in challenging scenarios but also enable finer-grained categorization of kick events into more detailed action types, such as passes, crosses, shots, and clearances.

GenAI Usage Disclosure

We used generative AI tools in a limited and supportive manner during the preparation of this manuscript. Specifically, we used ChatGPT 5.2 to improve the clarity and readability of the writing through phrasing and grammar refinement. In addition, we used Codex 5.2 to support data preprocessing, visualization, and debugging. All core research contributions, including the main ideas, methodology design, experiments, and analytical insights, were developed and validated entirely by the authors.

References

- [1] Michael A. Alcorn and Anh Nguyen. baller2vec++: A look-ahead multi-entity transformer for modeling coordinated agents. *arXiv preprint arXiv:2104.11980*, 2021.
- [2] Michael A. Alcorn and Anh Nguyen. baller2vec: A multi-entity transformer for multi-agent spatiotemporal modeling. *arXiv preprint arXiv:2102.03291*, 2021.
- [3] Anar Amirli and Hande Alemdar. Prediction of the ball location on the 2d plane in football using optical tracking data. *Academic Platform Journal of Engineering and Smart Systems*, 10(1):1–8, 2022.
- [4] Gabriel Anzer, Kilian Arnsmeyer, Pascal Bauer, Joris Bekkers, Ulf Brefeld, Jesse Davis, Nicolas Evans, Matthias Kempe, Samuel J. Robertson, Joshua W. Smith, and Jan Van Haaren. Common data format (CDF): A standardized format for match-data in football (soccer). *arXiv preprint arXiv:2505.15820*, 2025.
- [5] Manuel Bassek, Robert Rein, Hendrik Weber, and Daniel Memmert. An integrated dataset of spatiotemporal and event data in elite soccer. *Scientific Data*, 12(195), 2025.
- [6] Pascal Bauer, Gabriel Anzer, and Laurie Shaw. Putting team formations in association football into context. *Journal of Sports Analytics*, 9(6):39–59, 2023.
- [7] Alina Bialkowski, Patrick Lucey, Peter Carr, Yisong Yue, Sridha Sridharan, and Iain A. Matthews. Large-scale analysis of soccer matches using spatiotemporal tracking data. In *IEEE International Conference on Data Mining*, 2014.
- [8] Jonas Bischofberger, Arnold Baca, and Erich Schikuta. Event detection in football: Improving the reliability of match analysis. *PLOS ONE*, 19(4), 2024.
- [9] Paul S. Bradley and Jack D. Ade. Are current physical match performance metrics in elite soccer fit for purpose or is the adoption of an integrated approach needed? *International Journal of Sports Physiology and Performance*, 13(5):656–664, 2018.
- [10] Guillem Capellera, Luis Ferraz, Antonio Rubio, Antonio Agudo, and Francesc Moreno-Noguer. TranSPORTmer: A holistic approach to trajectory understanding in multi-agent sports. In *Proceedings of the 17th Asian Conference on Computer Vision*, 2024.
- [11] Guillem Capellera, Luis Ferraz, Antonio Rubio, Alexandre Alahi, and Antonio Agudo. JointDiff: Bridging continuous and discrete in multi-agent trajectory generation. In *Proceedings of the 14th International Conference on Learning Representations*, 2026.
- [12] Guillem Capellera, Antonio Rubio, Luis Ferraz, and Antonio Agudo. Unified uncertainty-aware diffusion for multi-agent trajectory modeling. In *IEEE/CVF Conference on Computer Vision and Pattern Recognition*, 2025.
- [13] Han-Jun Choi, Hyunsung Kim, Minho Lee, Minchul Jeong, Changjo Kim, Jinsung Yoon, and Sang-Ki Ko. Trajectory imputation in multi-agent sports with derivative-accumulating self-ensemble. In *Joint European Conference on Machine Learning and Knowledge Discovery in Databases*, 2025.
- [14] Fan R. K. Chung. *Spectral Graph Theory*, volume 92 of *CBMS Regional Conference Series in Mathematics*. American Mathematical Society, 1997.
- [15] Paolo Cintia, Salvatore Rinzivillo, and Luca Pappalardo. A network-based approach to evaluate the performance of football teams. In *ECML PKDD Workshop on Machine Learning and Data Mining for Sports Analytics*, 2015.
- [16] Filipe Manuel Clemente, Fernando Manuel Lourenço Martins, Dimitris Kalamaras, Daniel P. Wong, and Rui Sousa Mendes. General network analysis of national soccer teams in FIFA World Cup 2014. *International Journal of Performance Analysis in Sport*, 15(1):80–96, 2015.
- [17] Tom Decroos, Lotte Bransen, Jan Van Haaren, and Jesse Davis. Actions speak louder than goals: Valuing player actions in soccer. In *Proceedings of the 25th ACM SIGKDD Conference on Knowledge Discovery and Data Mining*, 2019.
- [18] Tom Decroos and Jesse Davis. Player vectors: Characterizing soccer players' playing style from match event streams. In *Joint European Conference on Machine Learning and Knowledge Discovery in Databases*, volume 11908 of *Lecture Notes in Computer Science*, pages 569–584. Springer, 2019.
- [19] Tom Decroos, Jan Van Haaren, and Jesse Davis. Automatic discovery of tactics in spatio-temporal soccer match data. In *Proceedings of the 24th ACM SIGKDD International Conference on Knowledge Discovery and Data Mining*, 2018.
- [20] Tom Decroos, Maaile Van Roy, and Jesse Davis. SoccerMix: Representing soccer actions with mixture models. In *Joint European Conference on Machine Learning and Knowledge Discovery in Databases*, 2020.
- [21] Ding Ding and H. Howie Huang. A graph attention based approach for trajectory prediction in multi-agent sports games. *arXiv preprint arXiv:2012.10531*, 2020.
- [22] David Douglas and Thomas Peucker. Algorithms for the reduction of the number of points required to represent a digitized line or its caricature. *Cartographica: The International Journal for Geographic Information and Geovisualization*, 10(2):112–122, 1973.
- [23] Jordi Duch, Joshua S. Waitzman, and Luís A. Nunes Amaral. Quantifying the performance of individual players in a team activity. *PLoS ONE*, 5(6):e10937, 2010.
- [24] Gregory Everett, Ryan J. Beal, Tim Matthews, Joseph Early, Timothy J. Norman, and Sarvapali D. Ramchurn. Inferring player location in sports matches: Multi-agent spatial imputation from limited observations. In *Proceedings of the 2023 International Conference on Autonomous Agents and Multiagent Systems*, 2023.
- [25] Dennis Fassmeyer, Pascal Fassmeyer, and Ulf Brefeld. Semi-supervised generative models for multiagent trajectories. In *Advances in Neural Information Processing Systems 35*, 2022.
- [26] Panna Felsen, Patrick Lucey, and Sujoy Ganguly. Where will they go? Predicting fine-grained adversarial multi-agent motion using conditional variational autoencoders. In *European Conference on Computer Vision*, 2018.
- [27] FIFA. Semi-automated offside technology, 2022. <https://inside.fifa.com/innovation/world-cup-2022/semi-automated-offside-technology>, Accessed: Jan 21, 2026.
- [28] Saibo Geng, Martin Josifoski, Maxime Peyrard, and Robert West. Grammar-constrained decoding for structured NLP tasks without finetuning. In *Proceedings of the 2023 Conference on Empirical Methods in Natural Language Processing*, 2023.
- [29] Zhiyong He, Zanbo Wang, Wei Wei, Shanshan Feng, Xianling Mao, and Sheng Jiang. A survey on recent advances in sequence labeling from deep learning models. *arXiv preprint arXiv:2011.06727*, 2020.
- [30] Sepp Hochreiter and Jürgen Schmidhuber. Long short-term memory. *Neural Computation*, 9(8):1735–1780, 1997.
- [31] Chris Hokamp and Qun Liu. Lexically constrained decoding for sequence generation using grid beam search. In *Proceedings of the 55th Annual Meeting of the Association for Computational Linguistics*, 2017.
- [32] S. K. Hong and Jae-Gil Lee. DTranNER: Biomedical named entity recognition with deep learning-based label-label transition model. *BMC Bioinformatics*, 21(1):53, 2020.
- [33] Zhiheng Huang, Wei Xu, and Kai Yu. Bidirectional LSTM-CRF models for sequence tagging. *arXiv preprint arXiv:1508.01991*, 2015.
- [34] Harry Hughes, Michael Horton, Xinyu Wei, Harshala Gammulle, Clinton Fookes, Sridha Sridharan, and Patrick Lucey. Event2Tracking: Reconstructing multi-agent soccer trajectories using long-term multimodal context. In *Proceedings of the 39th AAAI Conference on Artificial Intelligence*, 2025.
- [35] Geonhee Jo, Miru Hong, Han-Jun Choi, Minho Lee, Pascal Bauer, and Sang-Ki Ko. Imputing multi-agent trajectories from event and snapshot data in soccer. In *Proceedings of the 34th ACM International Conference on Information and Knowledge Management*, 2025.
- [36] Wonwoo Ju, Dominic Doran, Richard Hawkins, Antonio Gómez-Díaz, Andres Martín-Garcia, Jack D. Ade, Andy Laws, Mark Evans, and Paul S. Bradley. Contextualised peak periods of play in English Premier League matches. *Biology of Sport*, 39(4):973–983, 2022.
- [37] Hyunsung Kim, Han-Jun Choi, Chang Jo Kim, Jinsung Yoon, and Sang-Ki Ko. Ball trajectory inference from multi-agent sports contexts using set transformer and hierarchical bi-LSTM. In *Proceedings of the 29th ACM SIGKDD International Conference on Knowledge Discovery and Data Mining*, 2023.
- [38] Hyunsung Kim, Youyoung Choi, Sangwoo Seo, Tom Boomstra, Jinsung Yoon, and Chanyoung Park. ELASTIC: Event-tracking data synchronization in soccer without annotated event locations. In *ECML PKDD Workshop on Machine Learning and Data Mining for Sports Analytics*, 2025.
- [39] Hyunsung Kim, Gun-Hee Joe, Jinsung Yoon, and Sang-Ki Ko. Contextual sprint classification in soccer based on deep learning. In *IJCAI Workshop on Intelligent Technologies for Precision Sports Science*, 2024.
- [40] Hyunsung Kim, Bit Kim, Dongwook Chung, Jinsung Yoon, and Sang-Ki Ko. SoccerCPD: Formation and role change-point detection in soccer matches using spatiotemporal tracking data. In *Proceedings of the 28th ACM SIGKDD Conference on Knowledge Discovery and Data Mining*, 2022.
- [41] John D. Lafferty, Andrew McCallum, and Fernando C. N. Pereira. Conditional random fields: Probabilistic models for segmenting and labeling sequence data. In *Proceedings of the 18th International Conference on Machine Learning*, 2001.
- [42] Guillaume Lample, Miguel Ballesteros, Sandeep Subramanian, Kazuya Kawakami, and Chris Dyer. Neural architectures for named entity recognition. In *Proceedings of the 2016 Conference of the North American Chapter of the Association for Computational Linguistics*, 2016.

Computational Linguistics: Human Language Technologies, 2016.

[43] Juho Lee, Yoonho Lee, Jungtaek Kim, Adam R. Kosiorek, Seungjin Choi, and Yee Whye Teh. Set Transformer: A framework for attention-based permutation-invariant neural networks. In *Proceedings of the 36th International Conference on Machine Learning*, 2019.

[44] Brian Lester, Daniel Pressel, Amy Hemmeter, Sagnik Ray Choudhury, and Srinivas Bangalore. Constrained decoding for computationally efficient named entity recognition taggers. In *Proceedings of the 2020 Conference on Empirical Methods in Natural Language Processing*, 2020.

[45] Jiachen Li, Fan Yang, Masayoshi Tomizuka, and Chiho Choi. EvolveGraph: Multi-agent trajectory prediction with dynamic relational reasoning. In *Advances in Neural Information Processing Systems 33*, 2020.

[46] Jianhua Lin. Divergence measures based on the Shannon entropy. *IEEE Transactions on Information Theory*, 37(1):145–151, 1991.

[47] Daniel Link and Martin Hoernig. Individual ball possession in soccer. *PLOS ONE*, 12(7), 2017.

[48] Javier López Peña and Hugo Touchette. A network theory analysis of football strategies. In *Sports Physics: Proceedings of the 2012 Euromech Physics of Sports Conference*, pages 517–528, Palaiseau, France, 2012.

[49] Ximing Lu, Sean Welleck, Peter West, Liwei Jiang, Jungo Kasai, Daniel Khashabi, Ronan Le Bras, Lianhui Qin, Youngjae Yu, Rowan Zellers, Noah A. Smith, and Yejin Choi. NeuroLogic A*esque Decoding: Constrained text generation with lookahead heuristics. In *Proceedings of the 2022 Conference of the North American Chapter of the Association for Computational Linguistics: Human Language Technologies*, 2022.

[50] Patrick Lucey, Alina Bialkowski, Peter Carr, Stuart Morgan, Iain A. Matthews, and Yaser Sheikh. Representing and discovering adversarial team behaviors using player roles. In *IEEE Conference on Computer Vision and Pattern Recognition*, 2013.

[51] Patrick Lucey, Dean Oliver, Peter Carr, Joe Roth, and Iain A. Matthews. Assessing team strategy using spatiotemporal data. In *Proceedings of the 19th ACM SIGKDD International Conference on Knowledge Discovery and Data Mining*, 2013.

[52] Xuezhe Ma and Eduard H. Hovy. End-to-end sequence labeling via bi-directional LSTM-CNNs-CRF. In *Proceedings of the 54th Annual Meeting of the Association for Computational Linguistics*, 2016.

[53] Andrii Maksai, Xinchao Wang, and Pascal Fua. What players do with the ball: A physically constrained interaction modeling. In *IEEE Conference on Computer Vision and Pattern Recognition*, 2016.

[54] Weibo Mao, Chenxin Xu, Qi Zhu, Siheng Chen, and Yanfeng Wang. Leapfrog diffusion model for stochastic trajectory prediction. In *IEEE/CVF Conference on Computer Vision and Pattern Recognition*, 2023.

[55] Monnit Inc. Game-changing IoT sensors in 2022 World Cup soccer balls deliver real-time performance data, 2022. <https://www.monnit.com/blog/game-changing-iot-sensors-in-2022-world-cup-soccer-balls/>. Accessed: Jan 21, 2026.

[56] Alessio Monti, Alessia Bertugli, Simone Calderara, and Rita Cucchiara. DAG-Net: Double attentive graph neural network for trajectory forecasting. In *Proceedings of the 25th International Conference on Pattern Recognition*, 2020.

[57] Saul Needleman and Christian Wunsch. A general method applicable to the search for similarities in the amino acid sequence of two proteins. *Journal of Molecular Biology*, 48(3):443–453, 1970.

[58] Shayegan Omidshaefei, Daniel Hennes, Marta Garnelo, Zhe Wang, Adria Recasens, Eugene Tarassov, Yi Yang, Romuald Elie, Jerome T. Connor, Paul Muller, Natalie Mackraz, Kris Cao, Pol Moreno, Pablo Sprechmann, Demis Hassabis, Ian Graham, William Spearman, Nicolas Heess, and Karl Tuyls. Multiagent off-screen behavior prediction in football. *Scientific Reports*, 12(1):8638, 2022.

[59] Sean Papay, Roman Klinger, and Sebastian Padó. Constraining linear-chain CRFs to regular languages. In *Proceedings of the 10th International Conference on Learning Representations*, 2022.

[60] Marc Peral, Guillem Capellera, Luis Ferraz, Antonio Rubio, and Antonio Agudo. Multi-modal soccer scene analysis with masked pre-training. In *IEEE/CVF Winter Conference on Applications of Computer Vision*, 2026.

[61] Marc Peral, Guillem Capellera, Antonio Rubio, Luis Ferraz, Francesc Moreno-Noguer, and Antonio Agudo. Temporally accurate events detection through ball possessor recognition in soccer. In *Proceedings of the 20th International Joint Conference on Computer Vision, Imaging and Computer Graphics Theory and Applications*, 2025.

[62] Urs Ramer. An iterative procedure for the polygonal approximation of plane curves. *Computer Graphics and Image Processing*, 1(3):244–256, 1972.

[63] Jinchang Ren, James Orwell, Graeme A. Jones, and Ming Xu. Tracking the soccer ball using multiple fixed cameras. *Computer Vision and Image Understanding*, 113(5):633–642, 2009.

[64] Long Sha, Patrick Lucey, Yisong Yue, Peter Carr, Charlie Rohlf, and Iain A. Matthews. Chalkboarding: A new spatiotemporal query paradigm for sports play retrieval. In *Proceedings of the 21st International Conference on Intelligent User Interfaces*, 2016.

[65] Long Sha, Patrick Lucey, Stephan Zheng, Taehwan Kim, Yisong Yue, and Sridha Sridharan. Fine-grained retrieval of sports plays using tree-based alignment of trajectories. In *Proceedings of the 11th ACM International Conference on Web Search and Data Mining*, 2018.

[66] Fan-Yun Sun, Isaac Kauvar, Ruohan Zhang, Jiachen Li, Mykel J. Kochenderfer, Jiajun Wu, and Nick Haber. Interaction modeling with multiplex attention. In *Advances in Neural Information Processing Systems 35*, 2022.

[67] Zhiqing Sun, Zhuohan Li, Haoqing Wang, Di He, Zi Lin, and Zhi-Hong Deng. Fast structured decoding for sequence models. In *Advances in Neural Information Processing Systems 32*, 2019.

[68] Dung Thai, Sree Harsha Ramesh, Shikhar Murty, Luke Vilnis, and Andrew McCallum. Embedded-state latent conditional random fields for sequence labeling. In *Proceedings of the 22nd Conference on Computational Natural Language Learning*, 2018.

[69] Ashish Vaswani, Noam Shazeer, Niki Parmar, Jakob Uszkoreit, Llion Jones, Aidan N. Gomez, Łukasz Kaiser, and Illia Polosukhin. Attention is all you need. In *Advances in Neural Information Processing Systems 30*, pages 5998–6008, 2017.

[70] Ferran Vidal-Codina, Nicolas Evans, Bahaaeddine El Fakir, and Johsan Billingham. Automatic event detection in football using tracking data. *Sports Engineering*, 25(18), 2022.

[71] Andrew J. Viterbi. Error bounds for convolutional codes and an asymptotically optimum decoding algorithm. *IEEE Transactions on Information Theory*, 13(2):260–269, 1967.

[72] Xinchao Wang, Vitaly Ablavsky, Horesh Ben Shitrit, and Pascal Fua. Take your eyes off the ball: Improving ball-tracking by focusing on team play. *Computer Vision and Image Understanding*, 119:102–115, 2014.

[73] Tianwen Wei, Jianwei Qi, Shenghuan He, and Songtao Sun. Masked conditional random fields for sequence labeling. In *Proceedings of the 2021 Conference of the North American Chapter of the Association for Computational Linguistics: Human Language Technologies*, 2021.

[74] Wanneng Wu, Min Xu, Qiaokang Liang, Li Mei, and Yu Peng. Multi-camera 3d ball tracking framework for sports video. *IET Image Processing*, 14(15):3751–3761, 2020.

[75] Yi Xu, Armin Bazarjani, Hyung-Gun Chi, Chiho Choi, and Yun Fu. Uncovering the missing pattern: Unified framework towards trajectory imputation and prediction. In *IEEE/CVF Conference on Computer Vision and Pattern Recognition*, 2023.

[76] Raymond A. Yeh, Alexander G. Schwing, Jonathan Huang, and Kevin Murphy. Diverse generation for multi-agent sports games. In *IEEE/CVF Conference on Computer Vision and Pattern Recognition*, 2019.

[77] Jiaxuan You, Tianyu Du, and Jure Leskovec. ROLAND: Graph learning framework for dynamic graphs. In *Proceedings of the 28th ACM SIGKDD Conference on Knowledge Discovery and Data Mining*, 2022.

[78] Eric Zhan, Stephan Zheng, Yisong Yue, Long Sha, and Patrick Lucey. Generating multi-agent trajectories using programmatic weak supervision. In *Proceedings of the 7th International Conference on Learning Representations*, 2019.

[79] Shuai Zheng, Sadeep Jayasumana, Bernardino Romera-Paredes, Vibhav Vineet, Zhizhong Su, Dalong Du, Chang Huang, and Philip H. S. Torr. Conditional random fields as recurrent neural networks. In *2015 IEEE International Conference on Computer Vision*, 2015.

A Forward and Viterbi Algorithms

In this section, we elaborate on the forward and Viterbi algorithms for Conditional Random Fields (CRFs) [41], which are adapted to handle hard structural constraints in the proposed PathCRF.

A.1 Forward Algorithm for Training

Recall that the total score of an edge sequence $\mathbf{e} = (e_1, \dots, e_T)$ is defined in Eq. 6 as:

$$S(\mathbf{e}) = f_1(e_1) + \sum_{t=2}^T (f_t(e_t) + \psi_t(e_{t-1}, e_t)). \quad (11)$$

where the emission scores $f_t(e_t)$ and the transition scores $\psi_t(e_{t-1}, e_t)$ are derived from the edge embeddings. Using this score, Eq. 9 defines the CRF loss as the negative log-likelihood of the ground-truth edge sequence $\mathbf{e}^* = (e_1^*, \dots, e_T^*)$ given the input trajectories \mathbf{X} :

$$\mathcal{L}_{\text{CRF}} = -\log p(\mathbf{e}^* | \mathbf{X}) = \log Z - S(\mathbf{e}^*). \quad (12)$$

To minimize \mathcal{L}_{CRF} , we must compute the partition function $Z = \sum_{\mathbf{e}'} \exp(S(\mathbf{e}'))$. Since summing over all possible sequences is computationally intractable, ($\mathcal{O}(|\mathcal{E}|^T)$ where \mathcal{E} is the set of edges), we use the forward algorithm to effectively compute $\log Z$ via dynamic programming.

Let $\alpha_t(e)$ be the forward variable, representing the log-sum-exp score of all partial sequences ending with edge e at time t :

$$\alpha_t(e) = \log \sum_{\mathbf{e}_{1:t}, e_t=e} \exp(S(\mathbf{e}_{1:t})). \quad (13)$$

The values of $\alpha_t(e)$ for $e \in \mathcal{E}$ and $t = 1, \dots, T$ are obtained via the following recursion, and $\{\alpha_T(e) : e \in \mathcal{E}\}$ at the last time step are used to calculate $\log Z$.

Initialization ($t = 1$). At the first time step, $\alpha_1(e)$ is simply the emit score of e :

$$\alpha_1(e) = f_1(e), \quad \forall e \in \mathcal{E}. \quad (14)$$

Recursion ($t = 2, \dots, T$). We compute $\alpha_t(e)$ by aggregating scores from the previous time step. In particular, to enforce the hard constraints defined in Section 2.3.2, we iterate only over the set of allowed previous edges $\mathcal{P}(e) = \{e' \in \mathcal{E} : (e', e) \in \mathcal{A}\}$:

$$\alpha_t(e) = f_t(e) + \log \sum_{e' \in \mathcal{P}(e)} \exp(\alpha_{t-1}(e') + \psi_t(e', e)). \quad (15)$$

Since a large negative score (e.g., 10^{-4}) is assigned to transitions not in \mathcal{A} , they are effectively excluded from the sum of exponential scores.

Termination. Finally, $\log Z$ is obtained as the log-sum-exp of the forward variables at the last time step T :

$$\log Z = \log \sum_{e \in \mathcal{E}} \exp(\alpha_T(e)). \quad (16)$$

This reduces the complexity to $\mathcal{O}(T \cdot |\mathcal{A}|)$, which is even smaller than the forward algorithm of standard dense CRFs with $\mathcal{O}(T \cdot |\mathcal{E}|^2)$ due to the sparsity of \mathcal{A} .

A.2 Viterbi Algorithm for Inference

During inference, our goal is to find the most probable edge sequence $\hat{\mathbf{e}} = \arg \max_{\mathbf{e}} S(\mathbf{e})$, which is equivalent to finding the sequence that maximizes the score $S(\mathbf{e})$.

Let $\delta_t(e)$ be the max-score variable, representing the highest score among all partial sequences ending with edge e at time t :

$$\delta_t(e) = \max_{\mathbf{e}_{1:t}, e_t=e} S(\mathbf{e}_{1:t}). \quad (17)$$

The values of $\delta_t(e)$ for $e \in \mathcal{E}$ and $t = 1, \dots, T$ are obtained via the following recursion, and the optimal sequence is extracted by backtracking the optimal predecessor from $t = T$ to $t = 1$.

Initialization ($t = 1$). At the first time step, $\delta_1(e)$ is simply the emit score of e :

$$\delta_1(e) = f_1(e), \quad \forall e \in \mathcal{E}. \quad (18)$$

Recursion ($t = 2, \dots, T$). We compute the maximum score reaching each edge e at t while recording the optimal predecessor of e in a backpointer table $\text{ptr}_t(e)$:

$$\delta_t(e) = f_t(e) + \max_{e' \in \mathcal{P}(e)} (\delta_{t-1}(e') + \psi_t(e', e)) \quad (19)$$

$$\text{ptr}_t(e) = \arg \max_{e' \in \mathcal{P}(e)} (\delta_{t-1}(e') + \psi_t(e', e)) \quad (20)$$

By restricting the search space to $\mathcal{P}(e)$, we ensure the selected path never contains illegal transitions.

Termination and backtracking. We first identify the edge with the highest score at the final time step:

$$\hat{e}_T = \arg \max_{e \in \mathcal{E}} \delta_T(e). \quad (21)$$

Then, we reconstruct the optimal sequence $\hat{\mathbf{e}} = \arg \max_{\mathbf{e}} S(\mathbf{e})$ by backtracking via the pointers:

$$\hat{e}_{t-1} = \text{ptr}_t(\hat{e}_t), \quad t = T, \dots, 2. \quad (22)$$

The resulting sequence $\hat{\mathbf{e}}$ is the globally optimal possession path under the learned constraints.

B Ablation Study on Loss Terms

To examine the impact of the auxiliary loss terms introduced in Eq. 10, we conduct an ablation study by selectively removing $\mathcal{L}_{\text{coarse}}$ and $\mathcal{L}_{\text{emit}}$ from the training objective, by setting $\lambda_1 = 0$ or $\lambda_2 = 0$. We perform this experiment on both Static and Dynamic Masked CRFs, and report the results in Table 5, where the best-performing configuration for each CRF variant is highlighted in **bold**.

In Section 3.4, the baseline comparison reported in Table 2 shows that edge-level accuracies remain largely similar across different structuring methods and performance differences mainly emerge at the event level. In contrast, Table 5 demonstrates that removing auxiliary losses significantly degrades the accuracy from the edge level, which leads to weaker event detection performance. This indicates that the auxiliary terms play a crucial role in guiding the backbone toward learning discriminative possession representations, thereby stabilizing CRF training and improving both edge selection and downstream event detection. Overall, these results confirm that auxiliary supervision is essential for achieving strong performance in our framework.

Table 5: Loss function ablation study on the test data.

CRF module	\mathcal{L}_{CRF}	$\mathcal{L}_{\text{coarse}}$	$\mathcal{L}_{\text{emit}}$	Edge accuracy	Sender accuracy	Receiver accuracy	Violation rate	Event precision	Event recall	Event F1
Static MCRF	✓	✓	✓	69.54%	80.29%	82.02%	0.00%	68.57% (1464/2135)	79.96% (1464/1831)	73.83%
	✓	✗	✓	66.96%	78.71%	80.32%	0.00%	62.66% (1453/2319)	79.36% (1453/1831)	70.02%
	✓	✓	✗	66.09%	78.07%	80.02%	0.00%	69.26% (1390/2007)	75.91% (1390/1831)	72.43%
	✓	✗	✗	65.41%	76.67%	78.86%	0.00%	66.19% (1339/2023)	73.13% (1339/1831)	69.49%
Dynamic MCRF	✓	✓	✓	69.64%	80.44%	82.28%	0.00%	73.18% (1435/1961)	78.37% (1435/1831)	75.69%
	✓	✗	✓	67.52%	78.12%	80.77%	0.00%	70.02% (1387/1981)	75.75% (1387/1831)	72.77%
	✓	✓	✗	65.77%	78.62%	79.08%	0.00%	67.48% (1361/2017)	74.33% (1361/1831)	70.74%
	✓	✗	✗	65.64%	76.82%	78.71%	0.00%	71.32% (1246/1747)	68.05% (1246/1831)	69.65%

C Related Work

C.1 Trajectory Modeling in Multi-Agent Sports

Modeling trajectories in fluid multi-agent sports such as soccer, basketball, and American football is challenging due to the highly dynamic and coordinated interactions among many agents. Moreover, since player have no semantic ordering, effective models must satisfy permutation-equivariance with respect to the input players. Early studies [26, 50, 64, 65, 78] relied on assigning tactical roles [7] and imposing a fixed ordering of players before applying sequence models. However, such ordering is fundamentally limited, as players cannot be consistently aligned into a single one-dimensional arrangement across diverse match situations. Subsequent work increasingly adopted Graph Neural Networks (GNNs) [24, 58, 75, 76], which naturally capture player interactions while preserving permutation-equivariance. Their variants based on graph attention [21, 25, 45, 56, 66] further improved expressiveness by adaptively weighting the influence of neighboring agents depending on the context. More recently, Transformer [69] or Set Attention [43] have become popular alternatives, as they enable fast tensorized computation leveraging the fixed maximum number of agents [1, 2, 10, 13, 34, 35, 37, 60], whereas GNNs rely on graph batching and sparse message passing which are often computationally less efficient.

From a task perspective, sports trajectory understanding can be broadly categorized into trajectory forecasting, trajectory imputation, ball trajectory inference, and state classification [10]. Among them, trajectory forecasting has inherent uncertainty and is often approached with generative models such as Variational Recurrent Neural Networks (VRNNs) [21, 25, 45, 56, 66, 76, 78] or diffusion-based formulations [11, 12, 54]. In contrast, ball trajectory inference [3, 10, 37, 60] and state classification [6, 10, 60, 61] are typically treated as deterministic problems, based on the intuition that ball dynamics and on-ball events are largely determined once player movements are fully observed. As a possession state classification framework, our work follows this deterministic perspective, but differs from prior studies by explicitly enforcing logical consistency between consecutive states through a CRF-based architecture.

C.2 Structured Sequence Inference

Structured sequence labeling involves assigning a label to each token of an input sequence while satisfying predefined structural or

grammatical constraints [29]. A canonical example is the Beginning-Inside-Outside (BIO) tagging scheme used in Named Entity Recognition (NER), where an ‘inside’ (I) tag can only follow either a ‘beginning’ (B) tag or another ‘I’ tag of the same entity. To explicitly model such dependencies, Huang et al. [33] employs a CRF [41] architecture on top of Bi-LSTMs [30] to globally optimize the label sequence rather than per-token local predictions. Subsequent work [42, 52, 79] further enhanced this framework by incorporating character-level representations via CNNs or RNNs to capture morphological features without manual feature engineering. Some studies [32, 68] have explored dynamically adapting transition probabilities based on the input context instead of static transition matrix to better capture their time-varying dependencies. Furthermore, several approaches [44, 59, 73] explicitly mask illegal transitions in the CRF architecture, thereby guaranteeing structurally valid outputs by construction.

More recently, constrained decoding has gained attention in the context of large language models (LLMs), where enforcing structural constraints during training is difficult due to the autoregressive formulation and the extremely large output spaces that make traditional CRFs intractable [67]. Instead, many approaches impose hard constraints directly at inference time [28, 31, 49], ensuring structurally valid outputs without modifying the underlying model.